# Highly-Reliable Fly-back-based PV Micro-inverter Applying Power Decoupling Capability without Additional Components

Hiroki Watanabe, Nagaoka University of technology, Japan, hwatanabe@stn.nagaopkaut.ac.jp
Jun-ichi Itoh, Nagaoka University of technology, Japan, Itoh@vos.nagaopkaut.ac.jp

## Abstract

This paper discusses a verification of an electrolytic capacitor-less PV micro-inverter aiming for high reliability and volume reduction. The inverters, which are connected to a single-phase AC grid, have a double-line-frequency power ripple. Thus, a bulky electrolytic capacitor is generally used in DC side. The proposed converter consists of the fly-back converter, the voltage source inverter (VSI), and small capacitor in the DC link part in order to achieve the power decoupling without the any additional component. In addition, the sensor less magnetizing current control is proposed in order to ensure the compatibility between the surge voltage and cost reduction. Furthermore, it is demonstrated that the discontinuous current mode (DCM) of the proposed fly-back converter has the great power decoupling effect in comparison with the continuous current mode (CCM). From the experimental result, the second-order harmonics in the DCM operation is reduced by 97% in comparison with that in the CCM operation.

## 1. Introduction

Recently, a photovoltaic (PV) system is actively researched as a sustainable power solution due to the attractive characteristics such as; flexibility, high-system efficiency, and low manufacturing cost. Thus the utilization of the micro-inverters promisingly become a trend for the future PV system instead of using large capacity inverters. In particular, the micro-inverter with the high reliability is required because a large number of converter units are adopted to the PV generation system. However, in the conventional PV system, the electrolytic capacitors are usually employed owing to the requirement of the large capacitance. These capacitor limits the life-time of the converter, which results in low reliability.

On the other hands, in the converter topologies for the micro-inverter, the fly-back converter has been studying for following advantages; (i) Simple configuration and low manufacture cost (ii) galvanic isolation (iii) high voltage boost-up (IV) small volume. In this case, the configuration with the fly-back converter and the unfolding bridge is the center of attention because the unfolding bridge is switched at the line-frequency and the switching loss can be reduced drastically in comparison with that of two-stage isolated DC/AC converter. However, the large electrolytic capacitor is required in order to compensate the double-line frequency power ripple owing to single-phase AC grid. As a result, the life-time of the converter is limited due to the large buffer capacitor, which results in low reliability.

In order to solve this problem, the active power decoupling topologies for electrolytic capacitor-less converters have been researched actively [1]-[8]. The active power decoupling can reduce the capacitance for the double-line frequency power ripple compensation, which enables to use of film or ceramic capacitors instead of the electrolytic capacitor. However, the additional components such as the switching device and the passive components are required. Although the low cost is the one of the advantages of the fly-back micro-inverter, these components increase complexity of the circuit configuration and the cost.

This paper presents a simple configuration and the control method of the active power decoupling without any additional components. The proposed converter consists of the fly-back converter, the VSI and small buffer capacitor, which ensures the high reliability. In addition, the sensor less magnetizing current control is proposed in order to achieve the power decoupling capability. Owing to the proposed

control, the PV input current and the input power become constant. Furthermore, current sensor less control contributes the cost reduction.

This paper is organized as follows; first, the configuration of the conventional micro-inverter with fly-back converter is explained. Next, the proposed converter and a control block diagram are described. After that, the operation mode of the fly-back converter is considered focus on the power decoupling. Finally, the fundamental operation of the proposed converter is demonstrated by the simulation and experiment. From the experimental result, the second-order harmonics is reduced by 97% by the DCM operation. In addition, it is confirmed that the sinusoidal inverter output current.

## 2. Conventional fly-back micro-inverter topology

Figure 1 shows the typical configuration for the micro-inverter topology with a fly-back converter, and Figure 2 shows the fundamental operation waveforms of Fig.1. The primary side switch $S_1$ is switched at the high frequency in order to reduce the volume of the transformer. In this control, the duty command is adjusted to obtain absorb waveform with the grid frequency. After that, the secondary switch $S_2$ and $S_3$ is switched at the utility single-phase AC grid half cycle. On AC side, the small CL filter is connected in order to eliminate the switching frequency component. In this case, the switching loss of $S_2$ and $S_3$ can be reduced drastically because the switching frequency of the $S_2$ and $S_3$ is the same as the utility single-phase grid frequency.

One of the strong advantages in this configuration is a small number of the main circuit components. However, the bulky electrolytic capacitor $C_{buf}$ is required in the primary side of the transformer because the double-line frequency power ripple comes from the single-phase AC grid.

Figure 3 shows the micro-inverter topology with the conventional active power decoupling circuit [9]. In order to reduce the capacitance of $C_{buf}$, the small buffer capacitor $C_{apd}$ and the auxiliary circuit are added in the transformer secondary side. In this case, the $C_{apd}$ is charged and discharged in synchronized with the double-line frequency power ripple. As a result, the DC side capacitor $C_{buf}$ becomes small. However, these additional components complex the circuit configuration. In addition, the manufacturing cost will be increased

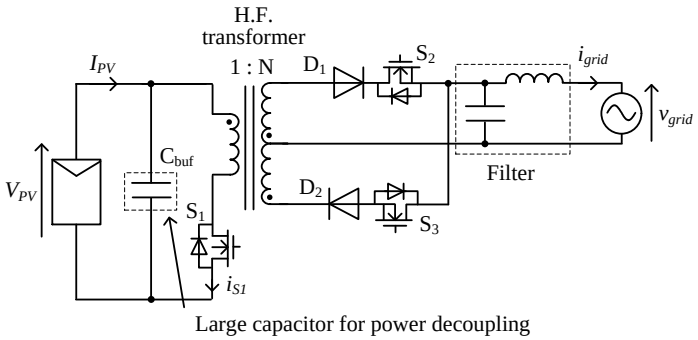


Fig. 1. Typically configuration of fly-back micro-inverter.

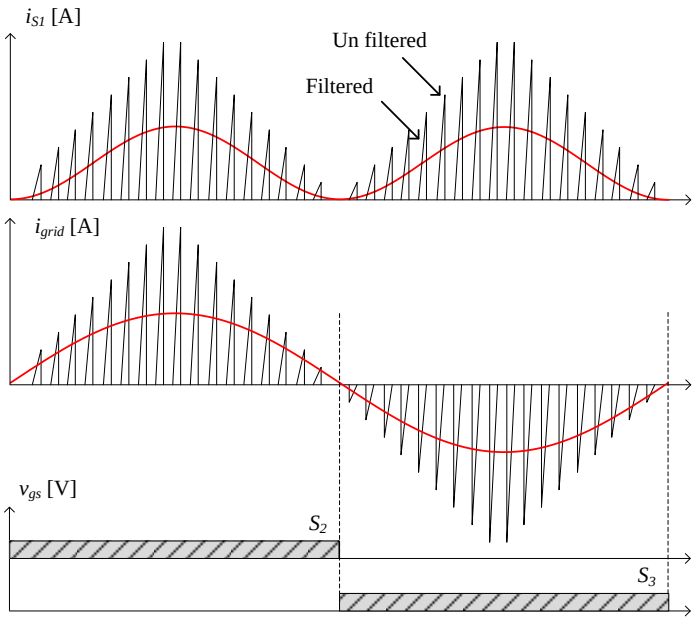


Fig. 2. Operation waveforms of typical fly-back micro-inverter in DCM. Sinusoidal modulation with PWM is applied on the primary side MOSFET, and the unfolder bridge $S_2$ and $S_3$ is switched at the line-frequency.

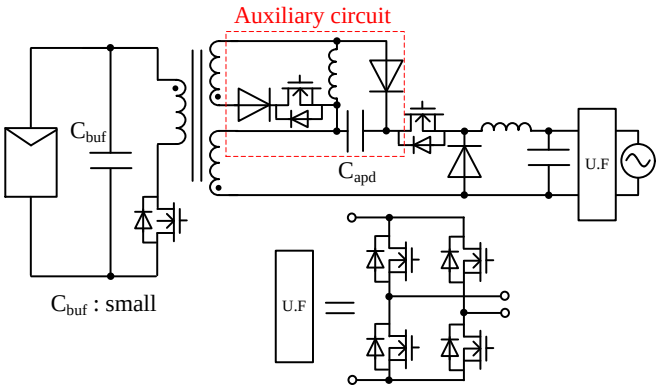


Fig. 3. Conventional fly-back micro-inverter with active power decoupling. It can reduce the capacitance of $C_{buf}$. However, auxiliary circuit is required, and expensive.

by the additional component for active power decoupling.

## 3. Proposed converter

Figure 4 shows the proposed converter which consists of the fly-back converter, the VSI and small buffer capacitor $C_{buf}$. The Fly-back converter isolates between the PV and the single-phase grid, and boosts the input voltage. After that, PV panel is connected to the single-phase grid by VSI. In the proposed converter, the double-line frequency power ripple is compensated by the $C_{buf}$, and the additional components such as the switching device and the passive components are not required in order to achieve the power decoupling. Thus, the proposed converter can reduce the cost and the volume of the converter in comparison with that of the conventional fly-back micro-inverter with the active power decoupling circuit as shown in Fig. 3.

Figure 5 shows the power decoupling strategy of the proposed converter. The unmatched power between the input and output power is compensated by the DC link capacitor. Figure 6 shows the principle of the power decoupling between the DC and single-phase AC sides. When both the output voltage and current waveforms are sinusoidal, the instantaneous output power $p_{out}$ is expressed as

$$p_{out} = \frac{V_{acp} I_{acp}}{2}(1 - \cos 2\omega t) \quad (1)$$

where $V_{acp}$ is the peak voltage, $I_{acp}$ is the peak current, and $\omega$ is the angular frequency of the output voltage. From (1), the power ripple that contains double-line frequency of the power grid, appears at DC link.

In order to absorb the power ripple, the instantaneous power $p_{buf}$ should be controlled by

$$p_{buf} = \frac{1}{2} V_{acp} I_{acp} \cos 2\omega t \quad (2)$$

where the polarity of the $p_{buf}$, is defined as positive when the buffer capacitor $C_{buf}$ discharges. Note that the active power of $C_{buf}$ should be zero. Owing to the power decoupling capability, the input power is matched to the output power. Thus, the relationship between the input and output power is expressed as

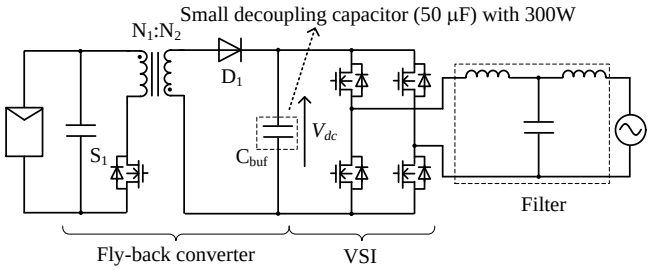


Fig. 4. Proposed converter with fly-back converter. The small buffer capacitor $C_{buf}$ compensates the double-line frequency power ripple. Thus, the additional component for power decoupling is not required.

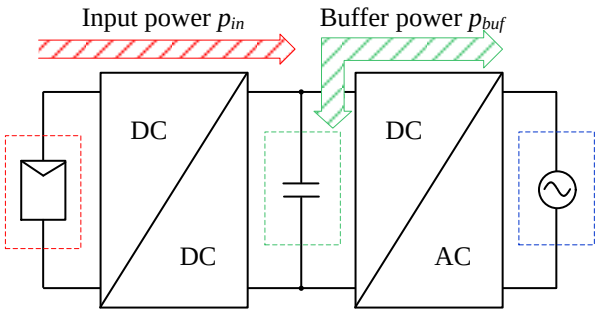


Fig. 5. Power decoupling strategy of the proposed converter.

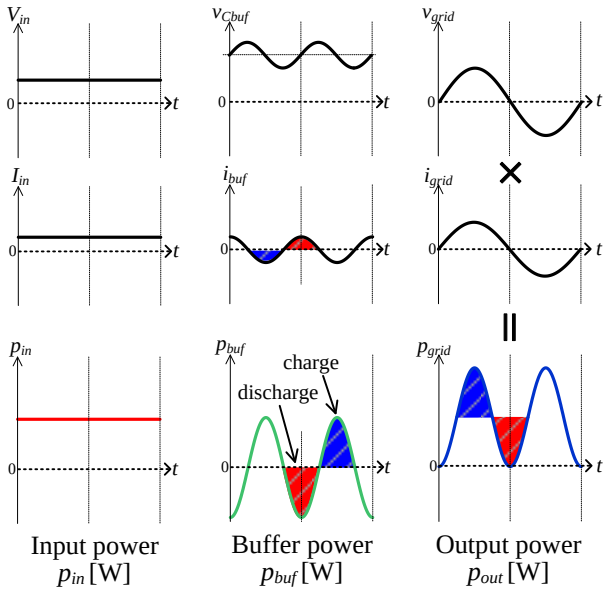


Fig. 6. Principle of the power ripple compensation. In order to obtain constant input power $P_{in}$, the buffer capacitor voltage $C_{buf}$ is fluctuated at the twice grid frequency.

$$p_{in} = \frac{1}{2} V_{acp} I_{acp} = V_{PV} I_{PV} \quad (3)$$

## 4. Operation mode of the fly-back converter focus on power decoupling capability

Figure 7 shows the primary current waveforms of the CCM and the DCM. When the MOSFET $S_1$ is turned on, the magnetizing inductor $I_m$ is charged. When the $S_1$ is turned off, the inductor energy is transferred to the secondary side through the diode of $D_1$.

Where, the average primary current both CCM and DCM is expressed as

$$I_{ave\_CCM} = \frac{V_{dc}}{V_{in}} I_{dc} \quad (4)$$

$$I_{ave\_DCM} = \frac{I_{peak}}{2} D_{on} \quad (5)$$

$$I_{peak} = \frac{V_{in}}{L_m} D_{on} T_{sw} \quad (6)$$

where, $I_{ave\_ccm}$ is the average primary current in CCM, $V_{dc}$ is the DC link voltage, $I_{dc}$ is the secondary input current, $V_{in}$ is the PV input voltage, $L_m$ is the magnetizing inductance, $D_{on}$ is the on-duty of $S_1$, $T_{sw}$ is the switching period.

Figure 8 shows the waveforms of the DC link voltage $V_{dc}$ and DC link current $I_{dc}$. From (4), in the CCM operation, the primary average current $I_{ave\_ccm}$ is decided from the $V_{dc}$ and $I_{dc}$. However, the $V_{dc}$ and $I_{dc}$ are fluctuated owing to the double-line frequency power ripple. Therefore, the cut-off frequency of the current regulator, which is enough higher than double-line frequency, should be designed. As a result, the $I_{ave\_ccm}$ is fluctuated, and it means the power decoupling is not achieved perfectly.

On the other hand, in the DCM operation, the primary average current is decided from the primary side parameter only from (6). Thus, the output side condition is not affected to the PV input side. As a result, the power decoupling operation is achieved consistently in the DCM operation. For these reason, the proposed circuit can apply the power decoupling operation in DCM with very simple operation.

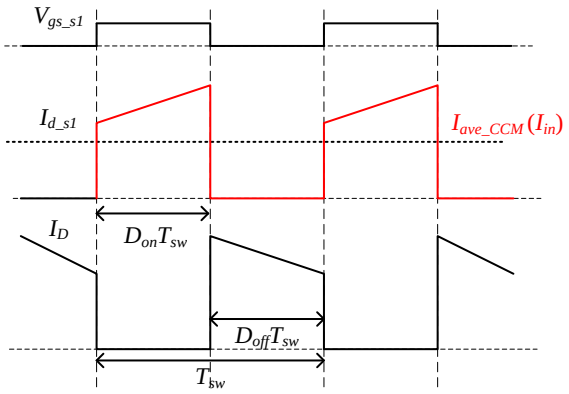


(a) CCM operation.

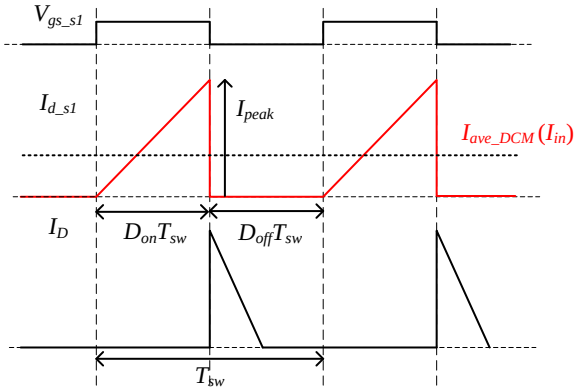


(b) DCM operation.

Fig.7. Primary current waveform.

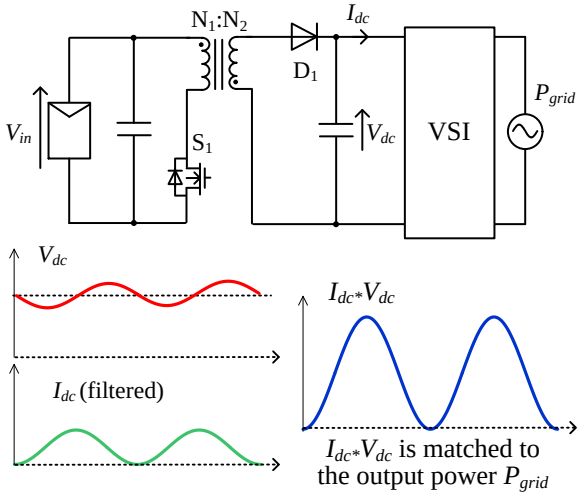


Fig. 8. Waveform of DC link voltage and current. In CCM operation, input power is affected to output power ripple because primary current is decided by DC link voltage and current.

## 5. Control block diagram

Figure 9 shows the control block diagrams of the proposed converter. In the fly-back control, the magnetizing current control is applied for power decoupling. When the fly-back converter is operated in CCM, the double-line frequency power ripple should be compensated in order to achieve the power decoupling. Note that the angular frequency of the power ripple is expressed as

$$\omega_{power\_ripple} = 4\pi f_{grid} \tag{8}$$

where, $f_{grid}$ is the grid frequency. In order to obtain the constant input power in CCM, the current command of the magnetizing current control $I_m$* is given by the constant value. In order to suppress the power ripple, the angular frequency of the current controller has to satisfy as (9)

$$\omega_{power\_ripple} << \omega_{acr} \tag{9}$$

Note that, when the fly-back converter is operated in DCM, the $\omega_{acr}$ can design low because the input power in the DCM is decided by only duty ratio of the switch $S_1$. Thus, in the DCM, the $\omega_{acr}$ is designed by the maximum power point tracking (MPPT), and it has the low response in comparison with the $\omega_{power\_ripple}$.

On the other hand, the proposed current control needs the parameter of the magnetizing current $I_m$. However, the current sampling is complicated because the $I_m$ has non-linear characteristics due to the flux saturation. In addition, when the wire inductance becomes high, it leads to the large surge voltage in the switch $S_1$. In order to solve this problem, the current sensor less control is developed.

Firstly, the ratio between the input and the output voltage of the fly-back converter is expressed as

$$\frac{V_{dc}}{V_{in}} = \frac{N_2}{N_1}\frac{d}{1-d} \tag{10}$$

where, $V_{dc}$ is the DC link average voltage, $V_{in}$ is the input voltage, $N_1$ and $N_2$ is the number of turns of the transformer, $d$ is the on-duty of the switch $S_1$.

According to (10), $d$ is expressed as (11)

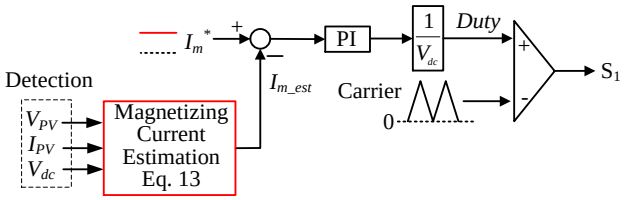


(a) Fly-back converter control

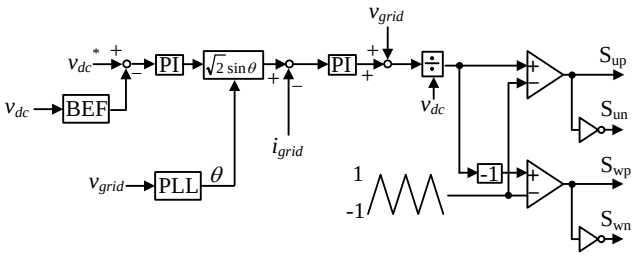


(b) VSI control

Fig. 9. Control block diagram.

$$d = \frac{1}{\frac{V_{in}}{V_{dc}}\frac{N_2}{N_1}+1} \tag{11}$$

On the other hand, the magnetizing current $I_m$ is expressed as

$$I_m = \frac{1}{1-d}\frac{N_2}{N_1}I_{dc} \tag{12}$$

where, $I_{dc}$ is the DC link current.

Finally, the estimation value of the magnetizing current $I_{m\_est}$ is expressed to (13) from (11) and (12)

$$I_{m\_est} = \frac{N_2}{N_1}\frac{\frac{V_{PV}}{V_{dc}}+1}{\frac{V_{PV}}{V_{dc}}}\frac{P_{PV}}{V_{dc}} = \frac{N_2}{N_1}\left(\frac{P_{in}}{V_{dc}}+I_{in}\right) \tag{13}$$

In expression (9), the $I_{dc}$ is calculated from the input power $P_{PV}$ and the DC link average voltage.

In the VSI control, the inverter output current control (ACR) and the DC link voltage control (AVR) are implemented in order to connect to the single-phase AC grid, and the DC link voltage command $V_{dc}$* in AVR is set more than the peak grid voltage $V_{acp}$. Note that, the DC link voltage has the double-line grid frequency component owing to the proposed decoupling control. As a result, the total harmonic distortion (THD) of the inverter

output current is decay. In order to solve this problem, a band eliminate filter is applied to the DC link voltage detection. The AVR controls the $V_{dc}$ by referring to the only average value of the DC link voltage.
Finally, the phase looked loop (PLL) is applied to ensure that the phase angle of the inverter output current is identical to the single-phase AC grid.

## 6. Simulation results

Table 1 shows the simulation parameters. Figure 10 shows the simulation results with the CCM operation. In the simulation, the operation of MPPT is not considered. The rated power is set to 300 W, and the buffer capacitor is 50 μF. In addition, the grid frequency is 50 Hz, and the angular frequency of the power ripple $\omega_{power\_ripple}$ is 625 rad/s.
According to Figure 10 (a) and (b), when the rate between the angular frequency of the ACR $\omega_{acr}$ and the $\omega_{power\_ripple}$ is low, the PV input current is fluctuated at the double-line grid frequency. On the other hand, when the $\omega_{acr}$ is increased to 4000 rad/s, the fluctuation of the PV input current becomes small. From these results, when the fly-back converter is operated in CCM, the $\omega_{acr}$ should be set more than the $\omega_{power\_ripple}$ in order to achieve the power decoupling capability. In addition, the inverter output current becomes sinusoidal waveform, and the buffer capacitor voltage $V_{dc}$ is fluctuated at the double-line grid frequency owing to the power decoupling. From these results, the validity of the fundamental operation of the proposed converter is confirmed.
Figure 11 shows the simulation results with the DCM operation. According to the Fig. 10 (a), when the $\omega_{acr}$ is set to 1000 rad/s, the PV input current has the double-line grid frequency component of 16.9%. However, According to the Fig. 11, the PV input current fluctuation is less than 1%. Following this result, it was confirmed that the power decoupling effect in DCM is larger than the CCM operation.
Figure 12 shows the comparison with the input current second-order harmonics with both the CCM and the DCM. In this case, the $\omega_{acr}$ is set to 4000rad/s. According to Fig.12, the second-order harmonics in DCM is less than the CCM operation. This is because the output side condition is not affected to the PV input power as shown in chapter 4.

Table.1 Simulation condition.

| Symbol | Quantity | value |
|---|---|---|
| $V_{PV}$ | Input voltage | 50 V |
| $P_{out}$ | Output power | 300 W |
| $f_{sw}$ | Switching frequency | 80 kHz |
| $C_{buf}$ | DC link capacitor | 50 μF |
| $L_m$ | Magnetizing inductor | 5 μH (200 μH) |
| $v_{ac}$ | Grid voltage | 200 $V_{rms}$ |
| $f_{ac}$ | Grid frequency | 50 Hz |

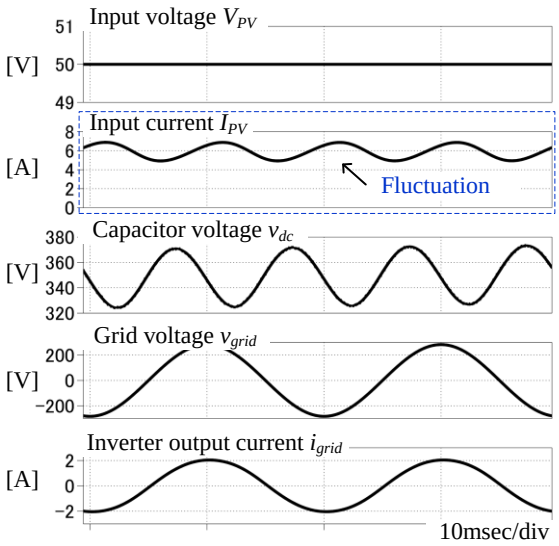


(a) $\omega_{acr}$ : 1000rad/s

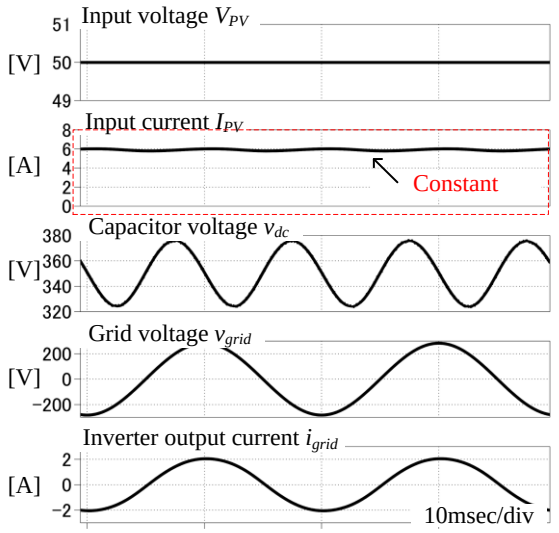


(b) $\omega_{acr}$ : 4000rad/s

Fig.10 Simulation results in CCM operation. When the angular frequency $\omega_{acr}$ increases, the input current becomes constant.

Figure 13 shows the characteristics of the power decoupling effect when the angular frequency of ACR $\omega_{acr}$ was changed. According to Fig.14, in the CCM operation, the second-order harmonics in the input current increase when the $\omega_{acr}$ is low. On the other hand, in the DCM operation, second-order harmonics is small at the all condition in comparison with the CCM operation. From these results, the DCM operation is validity in order to achieve the power decoupling.

## 7. Experimental results

In order to demonstrate the validity of the proposed decoupling method, a 300 W class prototype circuit is tested. Table 2 shows the experimental parameters, Figure 15 shows the experimental results with the CCM and DCM operation. In this experiment, the sensor loss current control is not applied because the purpose of this experiment is the comparison of the decoupling effect between the CCM and DCM operation. In addition, in order to clarify the difference between them, the fly-back converter is operated in the open loop control.

According to Fig. 14 (a), when the fly-back converter is operated in CCM, the input current is fluctuated at the double-line grid frequency. This is because the input current is affected from the output power ripple. It means the power decoupling is not achieved.

According to Fig. 14 (b), when the fly-back converter is operated in DCM, the input current fluctuation is reduced drastically in comparison with the CCM operation. From these results, the DCM operation of the fly-back converter has a power decoupling effect more than the CCM operation. Note that, this power decoupling operation is limited to the constant duty condition.

Figure 15 shows the comparison with the second-order harmonics on the input current. In the DCM operation, the second-order harmonics is reduced by 97% in comparison with that of the CCM operation. From these results, the validity of the proposed power decoupling is confirmed by this experiment.

## Conclusion

This paper presents a simple configuration and the control method of the active power decoupling without any additional components for fly-back micro-inverter. In order to achieve the power decoupling, the magnetizing current control is

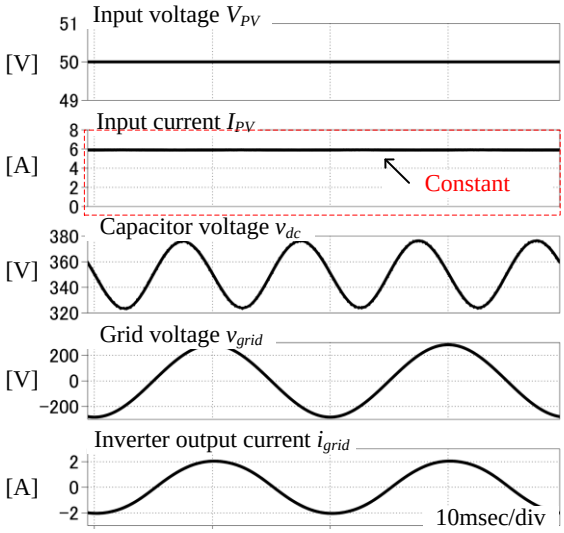


Fig.11 Simulation result in DCM operation when $\omega_{acr}$ is 1000rad/s. in the DCM operation, high speed response of $\omega_{acr}$ is not required.

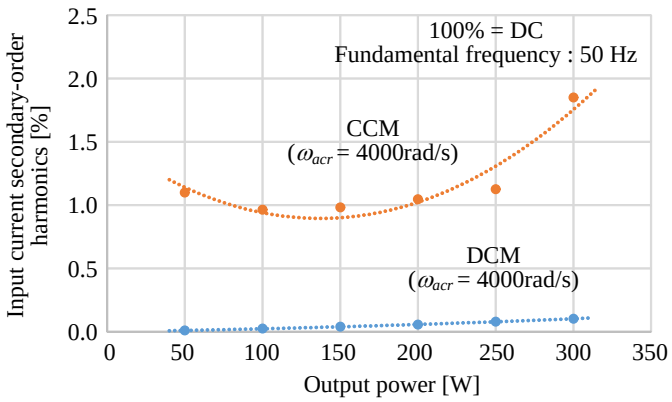


Fig.12 Comparison with the Input current second-order harmonics both the CCM and DCM.

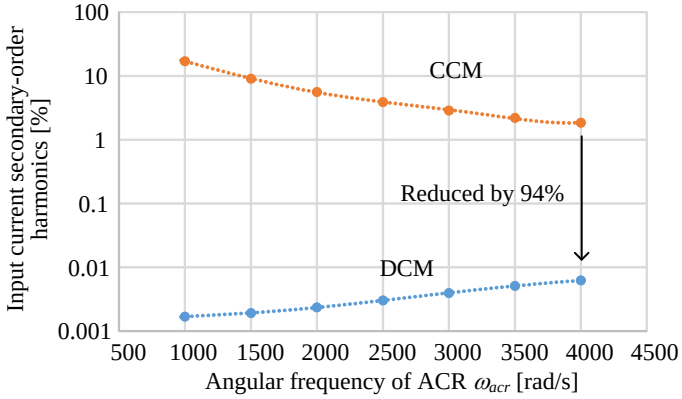


Fig.13 Characteristics of the power decoupling effect when the angular frequency of ACR was changed.

proposed. In addition, the operation mode of the fly-back converter for the power decoupling capability is explained. As a result, it was confirmed that the DCM operation has great effect for the power decoupling in comparison with that of the CCM operation. From the experimental result, the second-order harmonics is reduced by 97% in comparison with the CCM operation.
In the future work, some characteristics such as the efficiency and the converter loss will be demonstrated.

## Acknowledgment

This study was supported by New Energy and Industrial Technology Development Organization (NEDO) of Japan.

## Reference

[1] H. Renaudineau, S. Kouro, K. Schaible and M. Zehelein: “Flyback-based Sub Module PV Microinverter”, EPE`16 ECCE Europe, (2016)
[2] R-K. Surapaneni, A-K. Rathore: “A novel single-phase isolated PWM half-bridge microinverter for solar photovoltaic modules”, ECCE US pp. 4550-4556 (2015)
[3] E. Fonkwe, J. Kirtley, J. Elizondo: “Elyback micro-inverter with reactive power support capability”, IEEE 17th Workshop on Control and Modeling for Power Electronics (COMPEL), pp.1-8,(2016)
[4] F. Ji, L. Mu, G. Zhu: “A novel Multi-function photovoltaic Micro-inverter and its control strategy”, IEEE 8th International Power Electronics and Motion Control Conference (IPEMC-ECCE Asia), pp.1302-1305,(2016)
[5] S-M. Tayebi, C. Jourdan, I. Batarseh: “Dynamic Dead Time Optimization and Phase-Skipping Control Techniques for Three-Phase Micro-Inverter Applications”, IEEE transactions on Industrial Electronics, pp.1-10,(2016)
[6] Yoshiya Ohnuma, Jun-ichi. Itoh: “A Single-Phase Current-Source PV Inverter With Power Decoupling Capability Using an Active Buffer”,IEEJ transactions , Vol. 51, No. 1, pp. 531-538 (2015)
[7] X. Liu, M. Agamy, D. Dong,M. Harfman-Todorovic, L-Garces: “A low-cost solar micro-inverter with soft-switching capability utilizing circulating current”, IEEE Applied Power Electronics Conference and Exposition (APEC), pp.3403-3408,(2016)
[8] Y-M Chen, C-Y Liao: “A PV Micro-inverter with PV Current Decoupling Strategy”, IEEE transactions on Power Electronics, pp.1-14, (2016)

Table 2 Experimental parameter

| Symbol | Quantity | value |
|---|---|---|
| $P_{out}$ | Output power | 50 W |
| $f_{sw}$ | Switching frequency | 80 kHz |
| $C_{buf}$ | DC link capacitor | 40 μF |
| $L_m$ | Magnetizing inductor | 13 μH (DCM)<br>200 μH (CCM) |
| *Load* | R-L load | |
| $f_{ac}$ | Output frequency | 50 Hz |

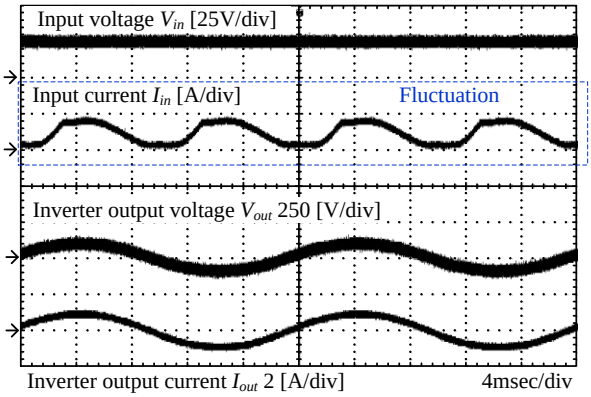


(a) CCM operation.

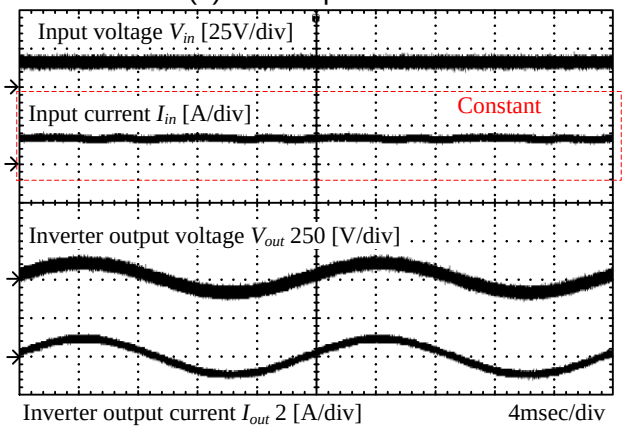


(b) DCM operation.

Fig. 14 Experimental results in order to evaluate power decoupling effect between CCM and DCM.

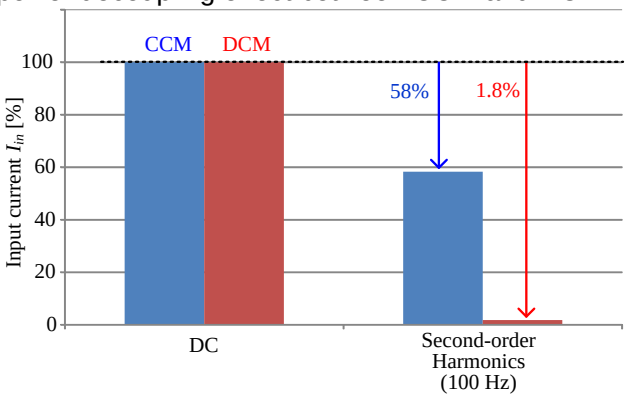


Fig. 15 Comparison with second-order harmonics on input current between the CCM and DCM.